Journal of Experimental Psychology:
Human Perception and Performance
1991, Vol. 17, No. 1, 183-197

0096-1523/91/$3.00

Steady-State and Perturbed Rhythmical Movements: A Dynamical Analysis

Bruce A. Kay
Department of Brain and Cognitive Sciences
Massachusetts Institute of Technology

Elliot L. Saltzman
Haskins Laboratories, New Haven, Connecticut

J. A. S. Kelso
Center for Complex Systems
Florida-Atlantic University

This study examined rhythmic finger movements in the steady state and when momentarily perturbed in order to derive their qualitative dynamical properties. Movement frequency, amplitude, and peak velocity were stable under perturbation, signaling the presence of an attractor, and the topological dimensionality of that attractor was approximately equal to one. The *strength* of the attractor was constant with increasing movement frequency, and the Fourier spectra of the steady-state trials showed an alternating harmonic pattern. These results are consistent with a previously derived nonlinear oscillator model. However, the oscillation was *phase advanced* by perturbation overall, and a consistent phase-dependent, phase-shift pattern occurred, which is inconsistent with the model. The overall phase advance also shows that any central pattern generator responsible for generating the rhythm must be nontrivially modulated by the limb being controlled.

The origin and form of biological rhythms have been the objects of intense inquiry for years, and many studies have focused on the neurophysiological bases of the oscillatory mechanisms (so-called central pattern generators, CPGs) that underlie such rhythms. For example, circadian rhythms (e.g., Pittendrigh & Daan, 1976) and rhythmic motor acts such as locomotion (Grillner & Zangger, 1979) have been studied in these terms. Much research into CPGs has been aimed toward answering the question: What is the actual form of a CPG in terms of neural structure and interactions among the component neurons, in particular behavioral and physiological situations (e.g., Carpenter & Grossberg, 1983; Lennard, 1985; Selverston, 1980)? However, because biological rhythms are so ubiquitous and occur over such a large variety of particular physical (e.g., neural or biochemical) structures, it is also important to look for macroscopic commonalities across these instantiations. This latter type of approach focuses on the more global, generic properties of the rhythmic behaviors themselves and complements more microscopic analyses.

In this article we report on the macroscopic dynamical properties of a simple, one-joint voluntary rhythmic movement. In a previous study (Kay, Kelso, Saltzman, & Schöner, 1987), we found that similar movements displayed an invariant relation between two basic parameters—frequency and amplitude—that characterize rhythm. We derived a simple dynamical model that could account for this relation. In that study, only steady-state rhythms were investigated, and only these basic kinematic parameters were studied. The purpose of the present article is to provide as complete and detailed a dynamical description of a rhythmic task as possible, both during steady-state rhythms and when the moving limb is momentarily perturbed. In developing a broader data base relevant to this class of movements, we also discuss more detailed, yet still abstract, models of how these movements might be generated and controlled.

Qualitative Dynamics

The approach adopted in our work for conceptualizing and modeling complex biological behavior is that of qualitative dynamics, an outgrowth of dynamical systems theory (e.g., Abraham & Shaw, 1982; Thompson & Stewart, 1986). Qualitative dynamics takes as data the evolution of a system's observable characteristics/descriptors and describes that evolution in terms of a set of equations of motion. The first step, prior to writing down any equations at all, is to classify the system's behavior qualitatively into generic categories or behavioral forms. As the data base is expanded, more refined and more quantitative statements are derived, including candidate dynamical equations and precise values for the equation's parameters. For example, the movement of a single limb to a target is described qualitatively as a point attractor.

An earlier version of this article was submitted in partial fulfillment of the doctoral degree program of Bruce A. Kay at the University of Connecticut, Storrs, Connecticut. The research reported herein was supported by Contract No. N00014-83-K-0083 from the U.S. Office of Naval Research and National Institute of Neurological and Communicative Disorders and Stroke Grant NS-13617. Preparation of this article was provided by Sloan Foundation Grant 87-2-16 to Bruce A. Kay.

We thank Arthur Winfree for comments on an earlier draft of the article, Paul Lennard for helpful discussion, and Esther Thelen, Gary Riccio, and two anonymous reviewers for their welcomed critiques.

Correspondence concerning this article should be addressed to Bruce A. Kay, who is now at the Department of Psychology, Brown University, Providence, Rhode Island 02912.

A point attractor is a stable equilibrium point that attracts all trajectories from arbitrary initial conditions. Point attractor dynamics have the property that a transient perturbation applied during movement does not deter achievement of the equilibrium point: Transient perturbation is equivalent dynamically to a resetting of initial conditions of the system's state variables (e.g., position and velocity). A simple example of point attractor dynamics is the damped linear mass-spring, describable by a second-order linear differential equation:

$$m\ddot{x} + \alpha\dot{x} + k(x - x_0) = 0, \quad (1)$$

where m is the mass, α the linear damping coefficient, k the linear stiffness coefficient, and x_0 the equilibrium position. In rhythmical tasks the appropriate qualitative dynamical description is a cycle. If the cycle is stable in certain respects, it is termed a periodic or limit-cycle attractor. A limit-cycle attractor, like a point attractor, attracts trajectories from arbitrary initial conditions, but a stable oscillation of fixed amplitude and frequency is attained. For the simplest oscillatory models, a suitable set of dynamical coordinates are position and velocity. These coordinates define a *phase space*, and in this space (here, the phase plane), the limit cycle is a closed loop or orbit. In addition to stable frequency and amplitude, the limit cycle's orbit can display characteristic scaling relations among its kinematic observables. For example, the well-known van der Pol oscillator (van der Pol, 1926) displays a constant amplitude across a wide range of oscillation frequencies and is described by the following second-order nonlinear differential equation:

$$m\ddot{x} + \alpha\dot{x} + \gamma(x - x_0)^2\dot{x} + k(x - x_0) = 0, \quad (2)$$

where γ is the coefficient of the nonlinear van der Pol damping term. In the closely related Rayleigh oscillator (Jordan and Smith, 1977), frequency and amplitude vary according to the inverse function. In both of these oscillators, the limit cycle's stability is due to the presence of nonlinear damping, or escapement, functions (Andronov & Chaikin, 1949; Kugler & Turvey, 1987; Kugler, Turvey, Schmidt, & Rosenblum, 1990; Minorsky, 1974).

In providing a qualitative dynamical account of rhythmical movements, we have investigated the following properties related to limit-cycle dynamics.

Presence of an Attractor

The first major property is that the behavior being modeled can be characterized as a limit-cycle *attractor*. Is an attractor actually present? This question can be answered by comparing kinematic variables such as frequency and amplitude before and after delivery of a transient mechanical perturbation.

Strength of the Attractor

Given the presence of an attractor, an important property is its strength of attraction. Trajectories perturbed away from limit cycles return more rapidly to strong attractors than to weak ones. Also, different oscillators have different functions relating attractor strength and various kinematic observables, such as frequency. For example, the strength of the van der Pol and other similar oscillators is constant across frequency and is constant regardless of where the oscillation is perturbed. The limit-cycle strength can be estimated by measuring the time taken for the system to return to the limit cycle following perturbation: Shorter returns to the limit cycle are associated with stronger attractors.

Phase Response Characteristics

An important descriptor of any rhythmic process is its phase response to perturbation (e.g., Stein, 1976; Winfree, 1980; Yamanishi, Kawato, & Suzuki, 1979). The question is whether the perturbation has the effect of shifting the rhythm in time with respect to an unperturbed, control rhythm. The amount of the shift is usually normalized to the period of the oscillation and is thus termed the phase shift. Phase shift patterns can be used to distinguish candidate oscillator models. For example, the sinusoidally forced linear damped mass-spring,

$$m\ddot{x} + \alpha\dot{x} + k(x - x_0) = F\cos(\omega t), \quad (3)$$

cannot be phase shifted by a mechanical perturbation to the mass. Following the transient, the mass resumes its preperturbation phase relation with the driver, which is unaffected by such perturbations. On the other hand, the van der Pol oscillator has no external driving term and can be phase shifted. Furthermore, it has a characteristic pattern of phase shift, depending on where in the cycle the motion is perturbed and also on the magnitude of the perturbation.

Dimensionality of the Attractor

A fourth property of a limit cycle is its dimensionality. The limit cycles that the Rayleigh and van der Pol oscilators produce are one-dimensional because they form a simple closed curve in the phase space: The motions are purely periodic. Oscillating biological systems are not ideal mathematical systems, however. They are never exactly periodic: When plotted on the phase plane, a rhythmic movement trajectory appears as a band around some average closed curve (see Figure 1a).

Is the variability we see due to a purely random, noisy process, or is another deterministic process present? If the variability is due to noise, then it may be modeled by the addition of a stochastic forcing function to the main oscillator equation; for example, the stochastic function may be interpretable as random fluctuations in the recruitment of motor units. On the other hand, the band of variability may be the result of an additional deterministic process; for example, a secondary oscillation having a frequency that is incommensurate with the larger scale oscillation may be present. Such a situation may reflect an interaction of central and peripheral oscillatory processes. In that case, the limit cycle is two-dimensional—one dimension for each oscillatory process—and is an example of a very different class of dynamical behavior, *quasi-periodicity*. A third way in which bands on the phase plane may be produced is by a deterministic *chaotic*

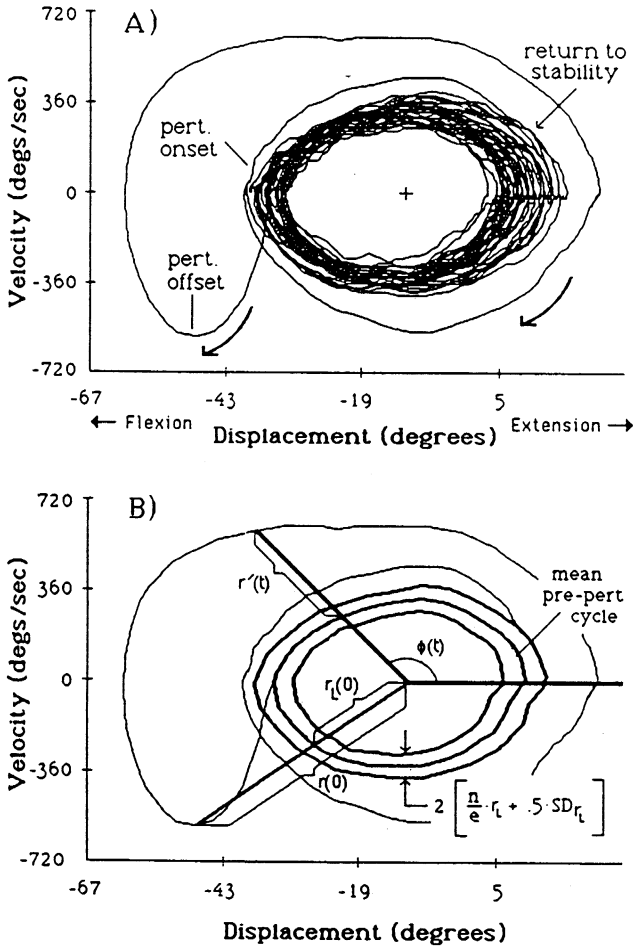

Figure 1. (a) Typical perturbation trial plotted on the phase plane. (The central cross indicates the location halfway between average preperturbation peak extension [more positive displacement values] and peak flexion [more negative]. (b) Notational conventions used in analyzing the response.

process (Thompson & Stewart, 1986), which exhibits trajectories that have fractional (or fractal; Mandelbrot, 1983) dimension. If the band of variability were to be produced by either of the deterministic methods, second-order dynamics would be inadequate. That is, second-order dynamics cannot generate two-dimensional limit cycle or chaotic attractors; the order of the dynamics must be third or greater (Thompson & Stewart, 1986). Such models are different at a fundamental level of qualitative dynamics from lower order models with added noise (which can be thought of as an additional infinite-dimensional process).

Thus, in order to distinguish among these three possibilities, one must assess the dimensionality of the attractor. Standard waveform analysis techniques cannot be relied upon to perform this task. The Fast Fourier Transform (FFT), for example, may not detect the presence of a second incommensurate frequency, if it is very close to the dominant frequency, and the spectrum of a chaotic system may be indistinguishable from that of stochastic noise (Bergé, Pomeau, & Vidal, 1984). In the present article, we use a computation that allows us to estimate the dimensionality of our movement trajectories directly (Grassberger & Procaccia, 1983; see Kay, 1988, for a tutorial on dimensionality analysis in the context of motor skills research).

Fourier Spectra of the Movement Trajectories

Although standard Fourier series methods do not afford a determination of the dimensionality of the attractors underlying the movement trajectories observed, they can provide key information regarding the structure of the dynamics producing such behaviors. All of the oscillators mentioned so far have characteristic spectra: The spectrum of the driven linear mass-spring has only one Fourier component, the fundamental, after decay of the initial transient. The van der Pol and Rayleigh oscillators' spectra contain a fundamental frequency and its odd harmonics, that is, the frequencies that are odd multiples of the fundamental. Their spectra contain much less energy in the even harmonics, and this is true for a very broad class of oscillators that contain certain symmetries in the structure of the dynamical equations. For example, the Rayleigh oscillator contains damping terms that are all in odd powers of the velocity ($\dot{x}$ and $\dot{x}^3$), and the damping function is symmetric about the origin $(x, \dot{x}) = (x_0, 0)$. Such a symmetry is mathematically termed odd symmetry. If even-powered damping terms are added, this symmetry is broken, and the spectrum contains even harmonics as well.

Preview of Methodology

In generating a broad descriptive base for rhythmic movements, we adopted two basic experimental protocols involving perturbation trials and steady-state trials. We used transient mechanical perturbations to test for the presence of an attractor, to measure the attractor strength, and to measure the system's phase response characteristics. In these trials, (a) the subject rhythmically cycled the index finger for several cycles, (b) the experimenter delivered a single torque-pulse perturbation, and (c) the subject continued cycling for several more cycles. Because of the great number of trials required for the phase response analysis, these trials were kept to a relatively short duration, 15 s to 25 s. In order to assess the dimensionality and Fourier spectrum of movement trajectories, the same subjects were required to perform steady-state (uninterrupted) trials of 50-s duration.

Method

Subjects

The subjects were 4 right-handed male volunteers; Subjects 2 and 4 were trained musicians (cellist and percussionist, respectively), whereas Subjects 1 and 3 had no musical training. Each subject participated in two experimental sessions, each session consisting of 3 hr of actual data collection.

Apparatus

The apparatus was a modification of one described in detail on previous occasions (Kelso, Holt, Rubin, & Kugler, 1981; see Figure

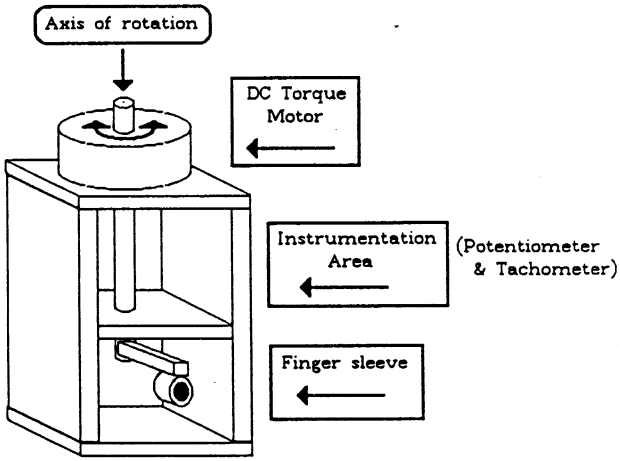

Figure 2. Schematic figure of the finger-positioning apparatus (instrumentation details omitted).

2). It consisted of a freely rotating finger manipulandum that allowed flexion and extension about the first joint (metacarpophalangeal) of the index finger in the horizontal plane. Two transducers were attached to the appratus's vertical rotation shaft: a precision DC potentiometer (which measured angular position of the finger) and a tachometer (which measured angular velocity). In addition, a DC torque motor was attached to the top of the shaft. The output signals of the transducers and the control voltage applied to the torque motor were recorded with a 16-track FM tape recorder for later digitization. The tachometer signal was also used in combination with threshold detection and delay circuitry to provide a trigger for delivering perturbations.

Procedure

Overall Experimental Protocol

Subjects were placed in a dentist's chair, and their right (dominant) forearm was placed in a preformed splint, which was rigidly attached to the finger-positioning device in such a way that the flexion–extension axis of the index finger's first joint was directly in line with the positioner's vertical axis. Vision of the finger was not excluded.

For all trials, we instructed subjects to cyclically flex and extend their index finger "at a confortable rate." They were not instructed explicitly about the amplitude of movement; for example, they were not told to move the finger maximally. For the steady-state trials, subjects were required to cycle continuously for a period of 1 min; 50 s from the middle portion of these trials were later analyzed.

Perturbation trials were conducted as follows: First, the subject started cycling, and, after a few cycles, would indicate to the experimenter if he was comfortable. The experimenter waited several more cycles, and then set the perturbation delivery process into motion (see next section). After the delivery of a perturbation, the experimenter collected several more cycles of data. A trial lasted from 15 to 25 s, depending on the subject's preferred tempo. Subjects were instructed not to actively resist the perturbation, but rather to try to return to a steady rhythm similar to that produced before the perturbation as quickly and as easily as possible.

Five blocks of trials, each consisting of 1 steady-state trial followed by 32 perturbation trials (a total of 165 trials), were collected in each session; each block lasted approximately 30 min.

Delivery of Perturbations

On every perturbation trial, a torque-pulse perturbation of one of two magnitudes (estimated at approximately 30 and 60 in-oz of torque) and directions (flexion or extension) was delivered by the DC torque motor. The pulse was 50 ms in duration and of constant amplitude.

In order to sample sufficiently the various portions of a movement cycle, we attempted to insert the perturbation in eight different angular sections on the phase plane, spaced at 45° intervals (see Figure 3). After initiation by the experimenter, external circuitry detected positive and negative peaks in the velocity signal, introduced one of four delays (zero, one-eighth, one-fourth, and three-eighths cycle period, plus a constant 30 ms), and triggered the appropriate torque pulse. For example, perturbations were delivered at approximately 0° by detecting a positive velocity peak and introducing a one-quarter period delay. The cycle period used to calculate each perturbation-trial block's phase delays was measured for the last few cycles of the immediately preceding steady-state trial. Thus, the set of delays that were used throughout a perturbation-trial block were specific to that block. All four combinations of perturbation magnitude and direction were delivered at each phase angle within each block.

Combining the two magnitudes, two directions, and eight phases of perturbation gave a total of 32 perturbation conditions. One trial of each of these conditions was collected in each block; order of presentation was randomized within each block. However, perturbation was not always delivered at the desired phase angle, because of false triggering (especially for the slower movements, which exhibited somewhat noisy velocity signals) and variations in cycle duration within and across trials. Also, a small number of perturbation trials (16 of 1,280) were lost because of experimenter error. Nevertheless, a wide scatter of phase locations was sampled (see Figure 3).

Data Reduction and Dependent Measures

Signal Processing

After the experimental sessions, the recorded transducer and torque control signals were played back and digitized at 200 samples/s, with

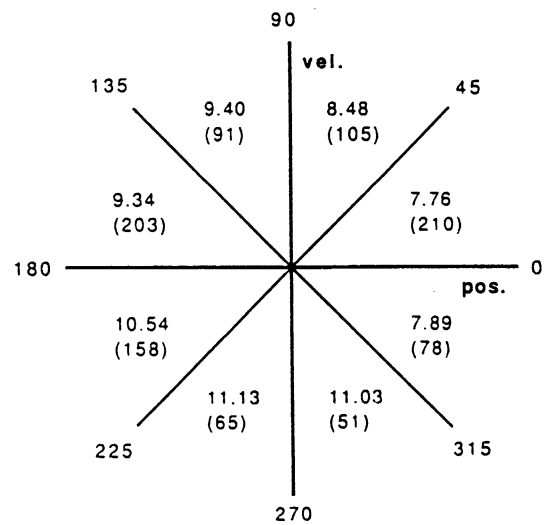

Figure 3. Phase-plane sectors used in perturbing the finger. (Numbers in parentheses are the total number of trials collected in each sector. Numbers outside parentheses are mean attractor strengths, σ, for the sectors.)

12-bit resolution. For the perturbation trials, the digitized position data were smoothed with a 35-ms (five sample) triangular window. In two of the eight sessions (Session 1 for Subjects 2 and 3), we experienced mechanical problems with the tachometer (although a good scatter of perturbations on the phase plane was still delivered), and so for these sessions, we computed angular velocity from the smoothed position data by using a two-point central difference algorithm. Both transduced and derived velocity data were smoothed with a 55-ms (nine sample) triangular window (see Kay, Munhall, V.-Bateson, & Kelso, 1985, for smoothing and differentiation details). The digitized torque control signal was used to locate the onsets and offsets of the torque pulses. All of the following analyses were performed on the digitized signals. An example of all three digitized signals is shown in Figure 4.

Perturbation Trial Measures

Kinematic measures: Frequency, amplitude, and peak velocity. For the perturbation trials, we measured frequency, amplitude, and peak velocity of movement cycles both before perturbation and after return to stable behavior following perturbation (see below for the return-to-stability criteria). A cycle was defined as the occurrence of two (successive) peak extension events, which, along with peak flexions, were identified by a peak-picking algorithm applied to the position data. Peak velocities were measured using the same peak-picker on the velocity data, for velocities of extension and flexion movements (positive and negative peaks, respectively. Cycle frequency (in Hz) was defined as the inverse of the time (in seconds) between two peak extensions, and cycle amplitude (peak-to-peak, in degrees) was defined as the average of the extension–flexion, flexion–extension half-cycle excursions. After obtaining these measures for each cycle, means and standard deviations across all steady-state cycles (pre- and post-perturbation) for each perturbation trial were obtained. The Results section reports these within-trial summary data, because of the large number of cycles collected (approximately 20,000).

Estimate of relaxation time and attractor strength. We displayed perturbation trials on the position-velocity phase plane in order to estimate the point at which the movement trajectory returned to stable rhythmic behavior (see Figure 1b). Two criteria had to be met simultaneously in order for the postperturbation rhythm to be termed *stable*: (a) the trajectory on the phase plane had to return within a band around the average preperturbation cycle and remain either inside of or reasonably near this band, and (b) the frequency of cycling had to settle to a stable value, whether or not that frequency was equal to the preperturbation frequency. The band of return was computed as follows: An average amplitude of the preperturbation oscillation on the phase plane, $r_L(\theta)$, was computed for each trial in each of 32 phase-plane sectors. The band of return was set to $[1 \pm n/e] \times r_L(\theta)$, plus one-half of its standard deviation. In this calculation, e is the base of the natural algorithm ($e = 2.717\ldots$), and the number n was chosen so that the trajectory was perturbed outside the band (n was set to 0.5 for most trials and to 0.25 for trials in which the perturbation had a smaller effect). The elapsed time between the offset of the perturbation and the time at which both of these criteria were first met was termed the relaxation time, T_{rel}. We found that frequency distributions of T_{rel} were positively skewed, typical of measurements constrained to be grater than zero. To perform statistical analyses, we used the log transform of the raw data; the reported results are the antilog transforms of the means so obtained.

The T_{rel} in theory can depend on how far the trajectory is perturbed from the limit cycle and therefore gives only an indirect indication of the attractor's strength. In order to measure more directly a limit-cycle attractor's strength, the actual form of the return process should be known a priori. Lacking that knowledge, we assumed that trajectories away from the limit cycle take the form of spirals winding back to the limit cycle, which is in qualitative accord with the appearance of our trajectories on the phase plane. That is, we assumed that the return process can be approximated by relaxation in amplitude only

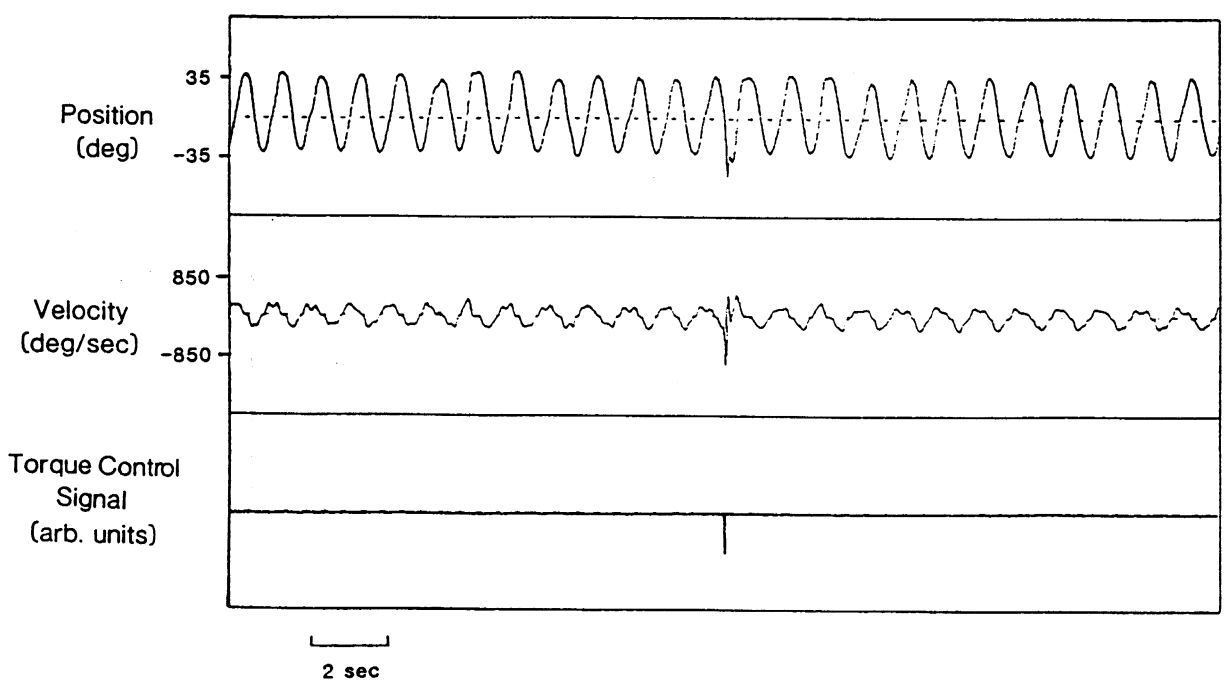

Figure 4. Time-series plot of a typical perturbation trial. (Top to bottom: angular displacement [extension = positive, flexion = negative], angular velocity, and the torque control voltage signal.)

(excluding, e.g., phase angle), which can be modeled by a first-order linear system displaying exponential decay. The return process was deemed to begin at the time of perturbation offset and end at T_{rel}. For each sample of the return process, the following expression for σ was computed (Figure 1b; see Appendix for details of σ's derivation):

$$\sigma = (1/t) \cdot \ln|[r(0) - r_L(0)]/[r(t) - r_L(t)]|, \quad (4)$$

where t is the elapsed time (in seconds) after the perturbation offset; $r(t)$ is the displacement from the center of oscillation of the return trajectory at time t; $r_L(t)$ is the average displacement of the preperturbation limit cycle in the same phase sector as the return trajectory at time t; and $r(0)$ and $r_L(0)$ are the same quantities, but measured at the moment of perturbation offset. The sample values of σ were averaged to provide a value for the entire return process. Like T_{rel}, the frequency distributions of σ were positively skewed; we applied the log transform to σ in order to perform statistical tests.

Phase response analysis. The phase of the new (postreturn) rhythm in relation to the old (preperturbation) rhythm was determined as follows (see also Winfree, 1980; Yamanishi et al., 1979): At peak extension events, the phase of the oscillation was defined as zero, and for all other points between peak extensions, phase = (t/T), where t is the time (in seconds) from the most recent peak extension to another event of interest, and T is the average preperturbation cycle period (in seconds). Thus, phase is not defined according to the phase angle on the phase plane. Rather, it is defined as a measure of relative temporal location within the cycle, normalized to units of cycle periods, $0 \leq$ phase < 1. The time at perturbation offset, t_p, was normalized as before by T to define the trial's old phase, ϕ. The elapsed time from the offset of perturbation to the first peak extension event following return to stable oscillation, t_θ, was measured and normalized to define the cophase of the new rhythm, θ. The temporal shift, Δt, was defined as $\Delta t = (t_p + t_\theta)$ (mod T), and normalized to define the rhythm's phase shift, $\Delta\phi = \Delta t/T = (\phi + \theta)$ (mod 1) and the new phase, $\phi' = (\phi + \Delta\phi)$ (mod 1; see Figure 5).

Thus, $\Delta\phi$ is the amount that the postperturbation rhythm has been phase-shifted in relation to the preperturbation rhythm, and ϕ' is the phase at which the perturbation would have been turned off in a new cycle if it were delivered at the same old phase in a control cycle (a cycle formed by the continuation of the average preperturbation rhythm). The computation is appropriate only if the pre- and postperturbation cycle periods agree exactly; however, because these numbers almost never exactly agreed, we accepted postperturbation deviations of ±5% from the preperturbation period (Yamanishi et al., 1979).

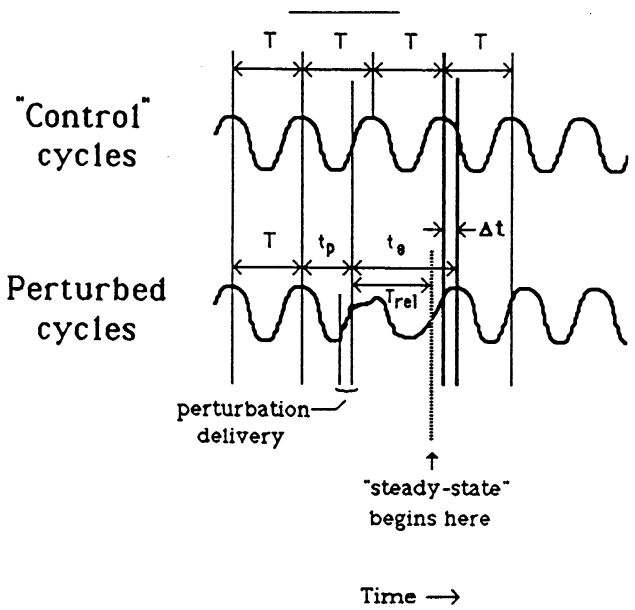

Figure 5. Conventions used in the phase response analysis. (Old phase $\phi = t_p/T$; cophase $\theta = t_\theta/T$; phase shift $\Delta\phi = \Delta t/T$.

To assess the pattern of phase shift that the rhythm exhibits, we constructed a phase transition curve (PTC), plotting new phase ϕ' versus old phase ϕ. Because this function is biperiodic, in the sense that ϕ' is a periodic function (with period 1) of ϕ and vice versa, a biperiodic function was used to curve-fit the data; standard linear regression techniques are inappropriate here because the arithmetic is actually being performed on the unit circle (Yamanishi et al., 1979). A least-squares fit was performed using the following function:

$$\phi'_{pred} = C_0 + a\phi + \sum_{k=1}^{2} [B_k \sin(2\pi k\phi) + C_k \cos(2\pi k\phi)], \quad (5)$$

where a is the overall linear slope of the function: c_0 is the intercept, which indicates the phase shift averaged across all old phases; and B_k and C_k are the weights on the sine and cosine terms. The error, E, to be minimized was defined as a function of the difference, d, between the measured ϕ' data and the estimated ϕ'_{pred}. Specifically, $d = (\phi' - \phi'_{pred})$ and

$$\begin{aligned} E &= d \quad \text{if} \quad -0.5 \leq d \leq 0.5 \\ &= d - 1 \quad \text{if} \quad d > 0.5 \\ &= d + 1 \quad \text{if} \quad d < -0.5. \end{aligned} \quad (6)$$

Thus, $-0.5 \leq E \leq 0.5$, preserving the distance relations between points on the unit circle. For example, with $\phi' = 0.9$ and $\phi'_{pred} = 0.1$, $d = 0.8$; however, these points are close together on the unit circle and $E = -0.2$ reflects this.

Steady-State Trial Measures

Dimensionality. We assessed the *correlation dimension* of the angular position time-series for the steady-state trials by computing the spatial correlation integral, $C(L)$ (Grassberger & Procaccia, 1983). Representing the data points of each steady-state trial as $x(i)$ ($i = 1, \ldots, N$; N = the number of data points), C was defined for each possible difference in angular position, L, between sample values as

$$C(L) = \lim_{N\to\infty} (1/N^2) \cdot |\#\ pairs\ [x(i), x(j)];\ |x(i) - x(j)| < L|, \quad (7)$$

where $i, j = 1, \ldots, N$; $i \neq j$; and $|x(i) - x(j)|$ is the Euclidean distance between angular position values. In the limit, as N approaches infinity,

$$C(L) = aL^{\nu}, \quad (8)$$

where a is an arbitrary constant and ν is the correlation dimension of the time series (Grassberger & Procaccia, 1983). This relation must hold over a finite range of distance values for the computation to be valid; that is, in a log-log plot, C and L should be linearly related over some values of L, where the slope of the line over that range is interpreted to be the correlation dimension.

In addition, $C(L)$ was computeed for a range of *embedding dimensions.* These computations entailed creating multidimensional vectors from time-shifted copies of the original single-dimensional time series as follows:

$$X(i) = [x(i), x(i + T), x(i + 2T), \ldots, x(i + (k - 1)T)], \quad (9)$$

where k is a positive integer indexing the embedding dimension, and T is a fixed number of samples of time delay. The standard higher dimensional Euclidean metrics were used in defining L for embedding dimensions $k > 1$. Embedding dimensions greater than one were used because the dimension of the underlying dynamics are a priori

unknown, and the computation is valid only when k is greater than or equal to the dimension of the dynamics (one criterion for k is that it must be at least $2\nu + 1$; Holzfuss & Mayer-Kress, 1986). For each embedding dimension, Equations 7 and 8 were used to compute $C(L)$ and ν.

For this data set, L, the intersample distance, ranged over 4,096 (2^{12}) discrete values for trials with maximal signal range; the average range was approximately three fourths of this range, or 3,072 discrete values. The L was further discretized into 256 distance bins for the actual correlation integral computation, so that $C(L)$ would have a sufficient number of data points for each bin. In addition, the 10,000-point records were down-sampled 4:1 to reduce the computational burden. The effective N for each trial was thus 2,500—a relatively small number for this kind of computation (see Abraham et al., 1986, for use of the algorithm with small data sets). We computed $C(L)$ for embedding dimensions 1 to 10 to ensure that k was much greater than $2n + 1$. An interdimension lag (T) corresponding to one fourth of the mean cycle period for each trial was used (Abraham et al., 1986; see Fraser & Swinney, 1986, for another criterion for picking lags). Across trials, this ranged from 6 to 32 samples.

A typical plot of $C(L)$ versus L, in logarithmic coordinates, is shown in Figure 6a. Plotting the local slope of this function versus L, a length interval over which the function approximated a straight line, was visually determined for each embedding dimension (i.e., where the slope was roughly constant; see Figure 6b). This scaling interval was about 25 distance bins wide in most cases. On this interval, the segment having the least-squared error for a linear fit of $\log(C(L))$ versus $\log(L)$ was found. The best-fit segment lengths were constrained to be greater than 5 distance bins and less than 25 distance bins in length (Kay, 1988). We then plotted the slope of the best-fit segment for each embedding dimension, interpreted as ν, as a function of embedding dimension (see Figure 6c for a typical plot) to see whether it converged to a stable value. Although this method of computing the correlation dimension does not afford an estimation of error, the cross-trial standard deviations of ν serve as a rough indication of error (see Holzfuss & Mayer-Kress, 1986, for direct error analysis methods).

Spectral analysis. The digital Fourier transform (DFT) was applied to the unfiltered position data from the steady-state trials. The 1,024-point DFT on the data revealed no significant spectral components (viz., above the noise floor) above 20 Hz. Subsequently, trials were down-sampled, to 5:1, to produce an effective Nyquist frequency of 20 Hz, and then a 1,024-point DFT was performed on the middle portion of the resultant 2,000-sample files (Figure 7).

Spectral peaks were determined visually on a high-resolution graphics screen, and their amplitudes calibrated to degrees. Because of the amount of data that could reasonably be collected in the perturbation trials, DFTs will not be reported on the steady-state portions of those trials; the spectral resolution was very poor in these much smaller data sets.

Results

Perturbation-Trial Data

In 300 of the trials in which the perturbation was delivered in the flexion direction, the finger hit the flexion stop-post (this never happened for extension-pulse trials). We eliminated these trials from the phase response and relaxation time analyses, because these computations rely on the precise nature of the system's transient behavior, which may have been obscured by this effect. The resultant N for these measures was 962 trials. In 19 trials, the initial displacement of the trajectory from the average preperturbation cycle [$r(0)$ −

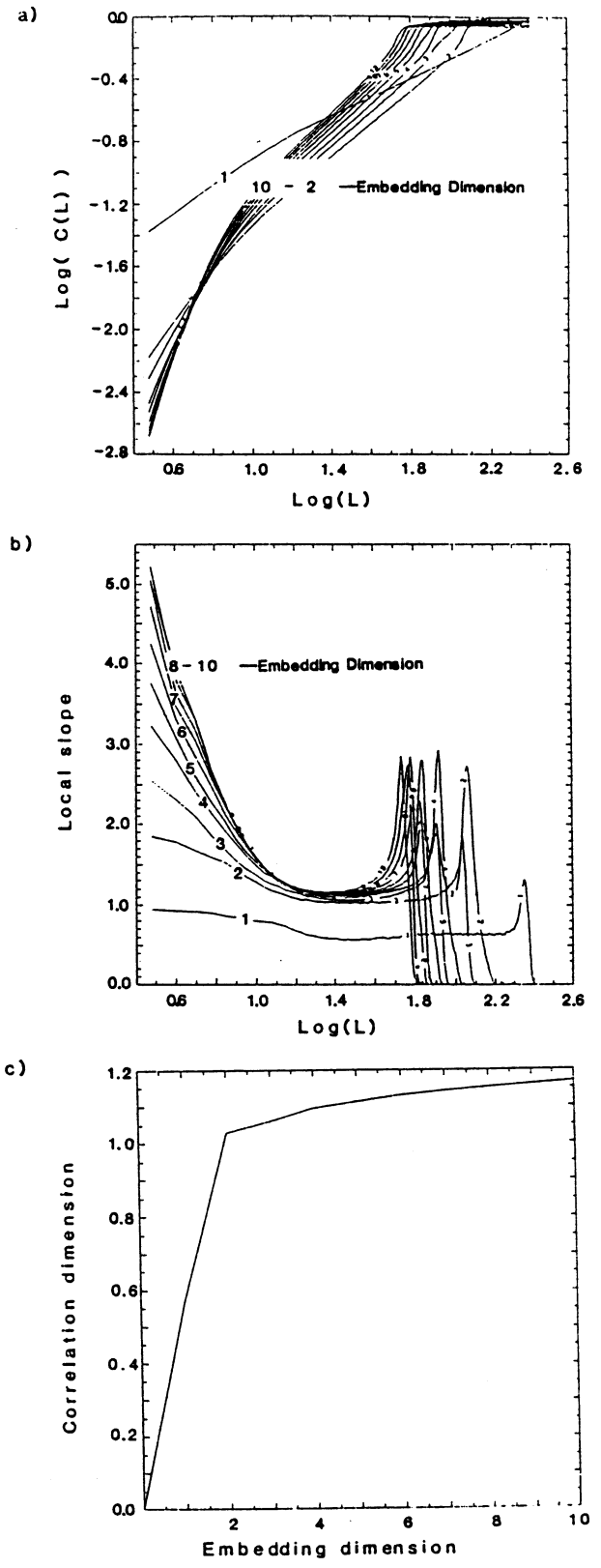

Figure 6. Typical dimensionality plots. (a) Logarithmic (base 2) plot of the spatial correlation integral (C; arbitrary units) versus distance (L; arbitrary units). (b) Local slope of the function in (A) versus $\log(L)$. (c) Computed correlation dimension (ν) versus embedding dimension (k).

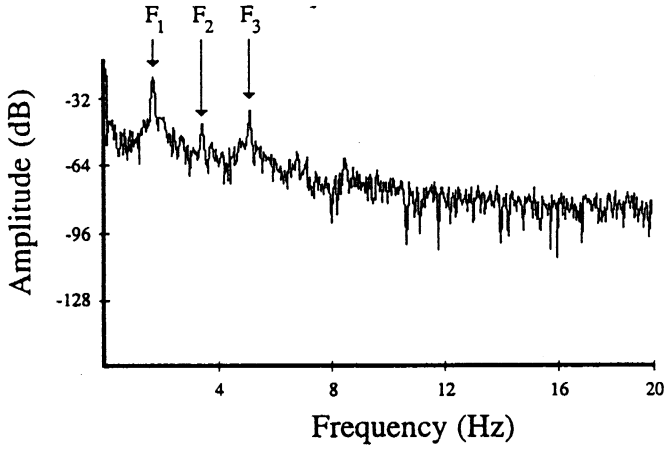

Figure 7. DFT plot for a typical steady state trial, from the down-sampled time-series (5:1), Nyquist frequency = 20 Hz.

$r_L(0)$] was less than all subsequently measured displacements; that is, the trajectory was perturbed too near the average preperturbation cycle to perform a measurement of σ. The N for this measure, then, was 943. All trials were retained, however, for the following analyses of the other kinematic observables (frequency, amplitude, and peak velocity), since only the steady-state portions of the trials are used for these analyses.

Stability of kinematic observables. Tables 1 and 2 present the average pre- and postperturbation values for within-trial frequency, amplitude, and peak velocity, averaged across all trials within each experimental session.

In 2 × 2 × 2 × 2 repeated-measures analyses of variance (ANOVAs), with session, perturbation direction (toward extension or flexion), perturbation magnitude (small or large), and time of measurement (pre- or postperturbation) as variables, no main effects of interaction were found for either frequency or amplitude. For peak velocity, a 2 × 2 × 2 × 2 × 2 ANOVA was performed, with the additional factor of cycle half (extension or flexion), and the only significant effects found were the Session × Time of Measurement two-way interaction, $F(1, 3) = 10.66$, $p < .05$, which was embedded within the four-way Session × Direction × Magnitude × Time of Measurement interaction, $F(1, 3) = 11.54$, $p < .05$, neither of which are of interest here. Overall, pre- and postperturbation values for all three kinematic observables were quite similar. In addition, there was no systematic difference between peak velocity going into extension and peak velocity going into flexion.

In summary, the stability of the kinematic observables of frequency, amplitude, and peak velocity indicate that a periodic attractor is indeed present.

Relaxation time and attractor strength. Table 3 lists mean relaxation time T_{rel} and attractor strength σ collapsed across all trials within each experimental session. A 2 × 2 × 2 ANOVA on T_{rel} with session, perturbation direction, and perturbation magnitude as variables revealed only a main effect of perturbation magnitude, $F(1, 3) = 192.71$, $p < .001$, with T_{rel} being longer for the stronger perturbations, averaging 551 ms, as opposed to 395 ms for the weaker pulses. Also, the range of T_{rel} values observed was not large—the range of the session means was only 204 ms whereas the range of mean cycle periods was 2,160 ms.

The same ANOVA on σ revealed significant main effects of session, $F(1, 3) = 24.70$, $p < .05$, and perturbation magnitude, $F(1, 3) = 48.18$, $p < .01$. The σ was smaller (indicating a weaker attractor) in the first session than the second (8.82 and 10.05, respectively), and was larger for the weak torque pulses than for the strong ones (10.10 and 8.58, respectively). The three-way Session × Direction × Magnitude interaction was also significant, $F(1, 3) = 36.91$, $p < .01$.

We performed one-way ANOVAs on T_{rel} and σ to determine how uniform each was with respect to the phase angle of perturbation onset. Observed onset angles were binned into eight sectors, 0°–45°, 45°–90°, . . ., 315°–360°. Phase angle had no effect on T_{rel}, $F(7, 21) = 1.09$, $p > .1$, but significantly affected σ, $F(7, 21) = 3.09$, $p < .05$. As can be seen in Figure 3, σ increases with increasing phase angle, starting from about 315° and going counterclockwise on the phase plane.

Table 1
Pre- and Postperturbation Frequency and Amplitude

	Frequency in deg.				Amplitude in deg.			
	Pre		Post		Pre		Post	
Subject	*M*	*SD*	*M*	*SD*	*M*	*SD*	*M*	*SD*
1								
Session 1	0.702	0.173	0.704	0.182	42.42	8.16	43.23	9.27
Session 2	0.379	0.042	0.363	0.078	46.79	4.67	41.74	14.76
2								
Session 1	0.692	0.109	0.687	0.116	73.84	3.48	74.91	3.85
Session 2	0.982	0.030	0.983	0.035	68.75	2.97	68.22	3.37
3								
Session 1	1.982	0.830	1.972	0.826	42.75	5.84	40.88	5.56
Session 2	0.830	0.053	0.826	0.053	54.97	9.27	54.81	9.87
4								
Session 1	0.527	0.088	0.528	0.084	55.67	4.05	55.06	3.67
Session 2	0.522	0.036	0.519	0.035	56.41	5.57	56.40	5.47
M	0.828	0.483	0.824	0.483	55.04	12.21	54.28	13.99

Table 2
Pre- and Postperturbation Peak Velocity (in degs/s)

	Extension				Flexion			
	Pre		Post		Pre		Post	
Subject	*M*	*SD*	*M*	*SD*	*M*	*SD*	*M*	*SD*
1								
Session 1	124.1	29.3	137.2	33.3	137.3	30.3	150.3	39.6
Session 2	79.0	19.4	79.4	24.0	88.2	19.3	87.8	26.9
2								
Session 1	155.5	29.2	159.1	31.3	178.7	38.2	181.9	40.0
Session 2	217.8	17.9	214.2	16.8	226.6	36.8	234.6	40.0
3								
Session 1	359.7	38.9	337.6	38.8	372.5	34.6	360.0	35.0
Session 2	263.5	93.8	253.4	84.9	251.0	83.8	240.4	72.1
4								
Session 1	178.3	36.6	181.8	36.9	139.9	35.0	145.5	38.6
Session 2	192.9	27.0	197.2	27.4	163.0	25.0	163.3	27.2
M	196.8	92.0	195.4	83.8	194.8	93.0	195.6	88.0

In order to assess how T_{rel} and σ scale with movement frequency, we performed correlations across all subject's data, because the range of observed frequencies within each subject's data was too small to allow such an analysis. The linear correlation of log(T_{rel}) and log(frequency) was not significant, $r(N = 961) = .05$, $p > .1$. The linear correlation of log(σ) and log(frequency) was also nonsignificant, $r(N = 943) = -.050$, $p > .1$.

In summary, neither relaxation time nor attractor strength were correlated with movement frequency; that is, both were effectively constant across the range of frequencies we observed. The range of T_{rel} values was rather small, and σ was not uniform on the phase plane.

Phase response. Only trials in which the mean postperturbation frequency differed from the mean preperturbation frequency by less than or equal to ±5% were used in this analysis. Of the 962 no-hit trials, 823 met this criterion. A typical phase transition curve (PTC); old phase ϕ vs. new phase ϕ') is shown in Figure 8, along with the data's best periodic fit. For each of the subjects' PTCs, the data tended to scatter around a line parallel to the $\phi' = \phi$ line.[1]

Table 3
Relaxation Time and Attractor Strength

Subject	T_{rel} (ms)	σ (1/s)
1		
Session 1	548	8.99
Session 2	418	10.13
2		
Session 1	488	9.15
Session 2	486	10.73
3		
Session 1	499	8.53
Session 2	344	9.89
4		
Session 1	437	8.62
Session 2	440	9.39
M	458	9.41

Accordingly, the linear slope parameter a in Equation 5 was fixed to 1.0, and the remaining parameters were determined by least-squares fitting. Three constrained multiple regressions were performed. First, the intercept was forced to zero, and the coefficients on the sine and cosine terms were obtained, as well as the overall R^2. The second regression fixed the sine and cosine terms to zero, leaving the intercept free to vary. The third fit was performed with all parameters (except slope) free to vary. Table 4 lists the intercepts found in the third fit and the R^2s for all three fits.

A paired t test comparing the R^2s of the first and third fits indicates that the intercept added significantly to the regression of new phase on old phase, $t(7) = 2.948$, $p < .05$. The intercept was always in the interval (0, .5), indicating that the postperturbation T_{rel} phase-led the control T_{rel}; that is, the phase response averaged across all old phases in all cases was a phase advance—no phase delays were observed.[2] The mean phase shift was 0.0750, significantly greater than zero, one-tailed $t(7) = 6.43$, $p < .01$. Incremental Fs (Kerlinger & Pedhazur, 1973) for each Subject × Session combination were all significant at the .05 level or better, range: $F(1, 106) = 4.82$ to $F(1, 123) = 86.45$.

Most of the flexion-pulse trials that were omitted from this analysis (due to subjects' hitting the stop) were delivered during the flexion portion of the cycle, and so these phases were somewhat underrepresented in the phase response analysis. Thus, the possibility exists that the fits obtained from the overall data set were biased. Accordingly, separate analyses (fits 1 and 3 described earlier) were carried out on the extension- and flexion-pulse data. In neither case did the paired t

[1] Winfree (1980) has termed this type of PTC Type 1 phase resetting, because the average slope of the PTC is 1. Another type of PTC occurs when the average slope is 0. In this case, the rhythm is strongly reset, in the sense that all information about the phase of perturbation is lost. Type 0 behavior did not occur in our experiment.

[2] Phases in this interval are conventionally termed advances, whereas in the interval (0.5, 1.0) they are termed delays (see Winfree, 1980, p. 145, Figure 14).

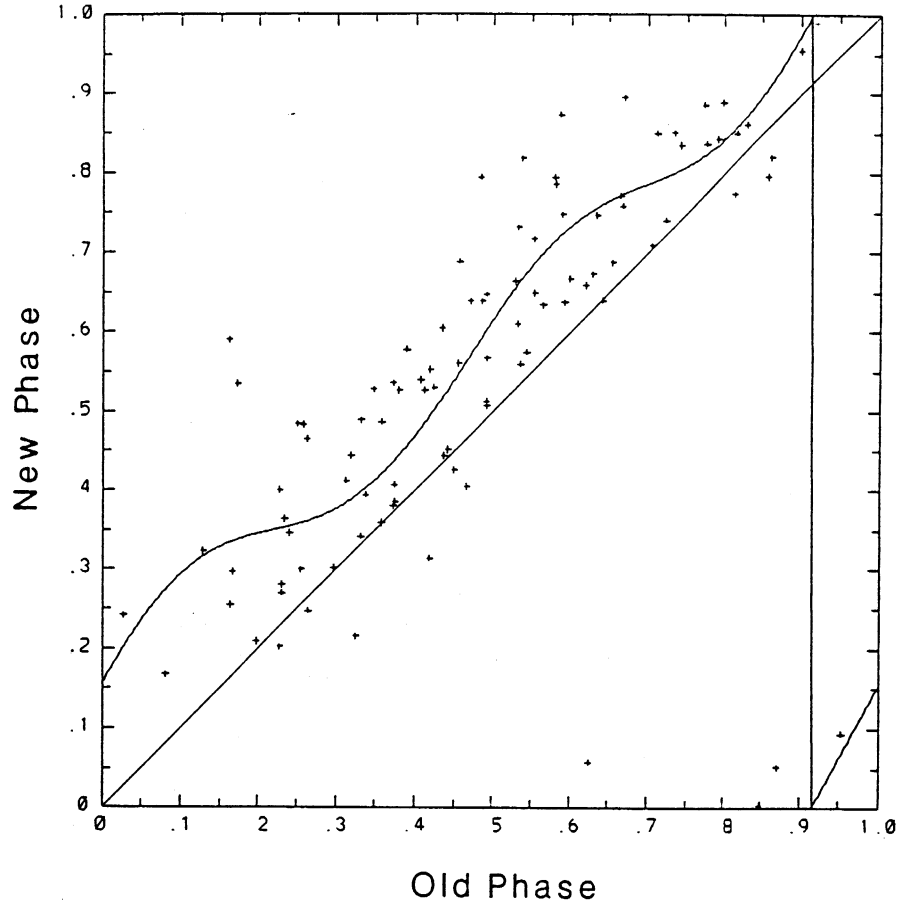

Figure 8. Phase transition curve data, and biperiodic fit, for Subject 2's Session 1 results.

test comparing the R^2s of fits 1 and 3 reach significance, $t(7) = 1.46$ and 1.67, for extension and flexion, respectively, probably because the Ns in these subanalyses were so low. However, for the extension-pulse data, in which few data points were eliminated, six of eight of the incremental Fs were significant, range: $F(1, 61) = 2.56$ to $F(1, 70) = 60.84$, and the corresponding overall phase shifts were phase advances. The two nonsignificant intercepts were also in the phase advance direction. For the flexion-pulse data, only three of eight incremental Fs reached significance, range: $F(1, 27) = 0.471$ to $F(1, 29) = 61.22$. Again, these were phase advances, and four of the remaining five intercepts were in the direction of phase advance. The only phase delay observed in the entire data set was nonsignificant. Phase advance did not depend on direction of perturbation, $t(7) = 0.86$, $p > .4$, averaging 0.0710 and 0.0596 for extension and flexion pulses, respectively, both of which were significantly greater than zero, one-tailed $t(7) = 5.99$, $p < .01$, and 3.14, $p < .05$, respectively.

Table 4
Coefficients of the Best Biperiodic Fits for Each Session

Subject	Intercept	R^2 fit 1	R^2 fit 2	R^2 fit 3
1				
Session 1	0.0631	.869	.882	.892
Session 2	0.0488	.895	.902	.923
2				
Session 1	0.1094	.662	.785	.812
Session 2	0.1030	.629	.612	.666
3				
Session 1	0.1217	.619	.768	.776
Session 2	0.0263	.848	.833	.855
4				
Session 1	0.0595	.882	.895	.916
Session 2	0.0681	.804	.793	.856

Similar results were obtained when the two perturbation-strength conditions were separately analyzed. A paired t test of the R^2s comparing fits 1 and 3 was significant for the weak condition, $t(7) = 2.58$, $p < .05$, but was not significant for the strong condition, $t(7) = 1.875$, $p > .1$. Six out of eight of the incremental Fs reached significance in both weak and strong conditions: weak range—$F(1, 55) = 0.315$ to $F(1, 52) = 58.28$; strong range—$F(1, 33) = 1.598$ to $F(1, 51) = 62.13$. The magnitude of the phase advance did not depend on perturbation strength, $t(7) = 0.43$, $p > .6$, with cross-subject means of 0.0675 and 0.0589 for the weak and strong perturbations, respectively, both of which were significantly greater than zero, one-tailed $t(7) = 4.73$, $p < .01$, and 2.95, $p < .05$, respectively.

In addition to the overall phase advance, there was a consistent phase-dependent pattern of phase shift, as revealed by the contributions of the sine and cosine terms. A paired t test comparing the R^2s of fits 2 and 3 was significant, $t(7) = 4.024$, $p < .01$). In six of the eight sessions, the incremental Fs were significant, range: $F(4, 106) = 2.448$ to $F(4, 86) = 9.554$. Collapsing the data across these six sessions, there were two old phases at which the phase advance reached local maxima, at $\phi = 0.22$ and $\phi = 0.67$. These correspond to about halfway through the flexion and extension half-cycles of movement, respectively. Furthermore, there were local minima at approximately $\phi = 0.4$ and $\phi = 0.96$, corresponding roughly to peak extension and peak flexion (see Figure 9).

The Ns for the extension- and flexion-pulse and weak- and strong-pulse data subsets were too small to allow separate analyses of phase-dependent patterns within these conditions, because of the large number of parameters in these fits.

In all of the results here, no differences were found between the nonmusicians (Subjects 1 and 3) and musicians (Subjects 2 and 4; cf. Yamanishi et al., 1979).

In summary, we found that the rhythm was consistently phase shifted overall (i.e., phase advanced across all sampled old phases) and that there was a consistent phase-dependent pattern of phase shift. Also, phase response did not depend on direction or magnitude of perturbation.

Steady-State Trial Data

Dimensionality. For all steady-state trials, the computed correlation dimension ν did not converge to a stable value with increasing embedding dimension, but rather continued to increase slightly, a pattern frequently observed in such analyses (Mayer-Kress, 1986; see Figure 6c). For a few trials, the computation was repeated for embedding dimensions $k = 1$ to 20, and the same lack of convergence occurred. Grassberger and Procaccia's (1983) algorithm is known to introduce systematic errors in the estimates of ν for high values of embedding dimensions (Mayer-Kress, 1986), but the embedding dimension used for the final determination of ν should be as large as possible, to ensure that it is larger than the dimension of the underlying dynamics. Mayer-Kress and Layne (1987) have recommended that the correlation dimension be measured from the results for $k = 7$, for low-dimensional attractors. Table 5 reports the within-session means and standard deviations of the computed correlation dimen-

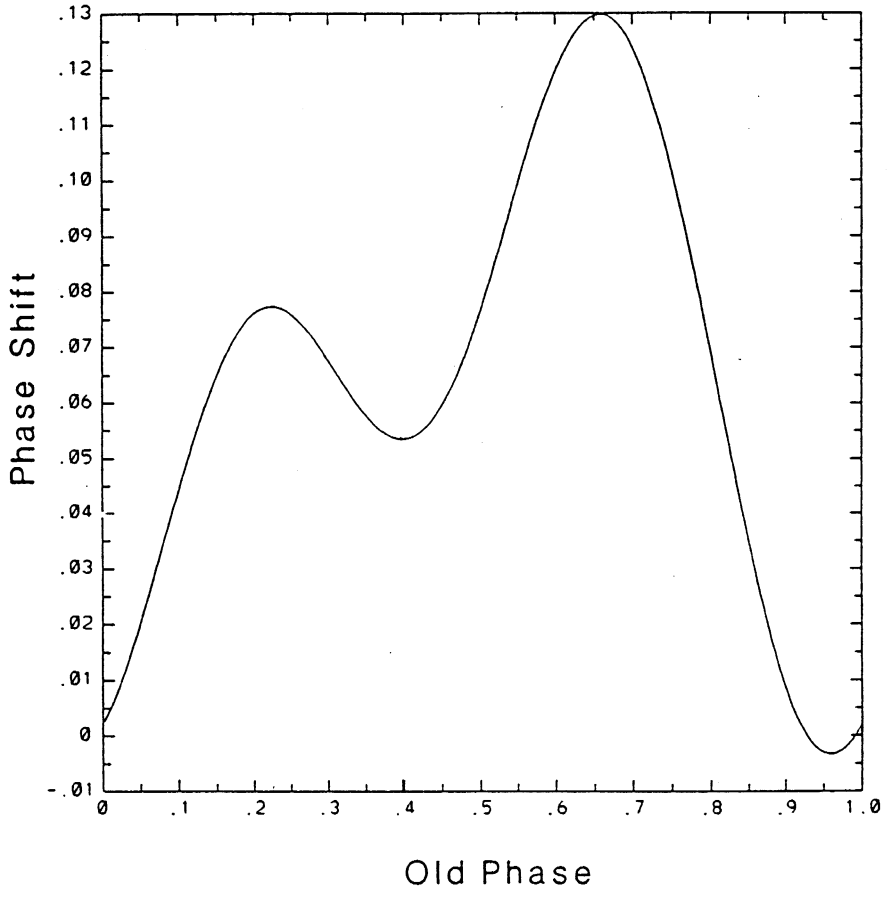

Figure 9. Phase shift ($\Delta\phi$) as a function of old phase (ϕ), for the biperiodic fit, across all sessions that showed a significant effect for sinusoidal components.

Table 5
Correlation Dimension, Scaling Interval, and Spectral Amplitudes of the Steady-State Trials

			Scaling interval (deg.)											
	ν		From		To		F_1 (deg.)		F_2 (deg.)		F_3 (deg.)		F_4 (deg.)	
Subject	*M*	*SD*	*M*	*SD*	*M*	*SD*	*M*	*SD*	*M*	*SD*	*M*	*SD*	*M*	*SD*
1														
Session 1	1.206	0.071	4.63	0.52	5.82	0.63	4.74	0.75	0.166	0.105	0.328[a]	0.117	0.052	0.049
Session 2	1.200	0.036	4.92	0.73	6.04	0.86	5.16	0.60	0.188	0.181	0.222	0.046	0.054	0.074
2														
Session 1	1.174	0.022	7.39	0.46	9.72	0.62	8.70	0.71	0.528	0.180	0.232	0.283	0.052	0.116
Session 2	1.182	0.036	7.51	0.57	9.24	0.36	8.14	0.79	0.376	0.242	0.112	0.157	0.000	0.000
3														
Session 1	1.199	0.045	5.34	0.50	7.20	0.68	5.56	0.88	0.154	0.095	0.382[a]	0.054	0.014	0.020
Session 2	1.103	0.128	6.36	1.21	8.37	1.08	7.58	1.39	0.066	0.148	1.088[a]	0.680	0.000	0.000
4														
Session 1	1.104	0.047	5.28	0.32	7.24	0.49	6.76	1.02	0.294	0.419	0.772[a]	0.280	0.114	0.110
Session 2	1.149	0.024	6.68	0.82	9.41	0.66	7.52	1.00	0.398	0.237	0.940[a]	0.055	0.224	0.135
M	1.165	0.068	6.01	1.12	7.88	1.53	6.77	1.44	0.271	0.156	0.510[b]	0.337	0.064	0.073

[a] $F_3 > F_2$, $p < .05$; [b] $F_3 > F_2$, $p < .01$.

sion ν and the scaling interval endpoints over which the computation was performed, for $k = 7$.

We performed 2 × 5 ANOVAs, with session and trial as variables, on ν and the interval endpoints; no effects or interactions were found. The observed ν values were similar to the value found for a sine wave with added quasi-random noise (1.20 ± 0.1, Abraham et al., 1986).[3] Note that the scaling intervals include the amplitudes of the fundamentals found in the spectral analysis (see Table 5). For amplitudes below the scaling interval, ν scaled linearly with embedding dimension; that is, it was approximately equal to k for all ks, indicating infinite-dimensional (e.g., stochastic) behavior for these short lenghths. For amplitudes above the scaling interval, the correlation integral $C(L)$ saturated, indicating zero-dimensional behavior at the largest scale (i.e., at the largest length scales, all behavior looks like a point attractor; Kay, 1988).

In summary, the dimensionality results indicate that the attractor is a low-dimensional one, consistent with a single oscillatory process at the medium length scales coexisting with a stochastic process at the smaller length scales.

Spectral analysis. Table 5 lists the amplitudes of the first four spectral peaks found in the dimension trials, averaged within session, from the fundamental F_1 to the fourth partial of the fundamental, F_4. All partials found were harmonically related to the fundamental (within the resolution of the DFT). The data exhibit relatively weak harmonic content, the sum of the amplitudes of F_2, F_3, and F_4 on average being only 12% of the amplitude of F_1. However, the third partial was greater in amplitude than the second, paired-trial $t(39) = 2.724$, $p < .01$.

In summary, the odd harmonics appear to predominate in the movements' spectra, consistent with the simple nonlinear oscillators discussed in the introduction.

Discussion

To a great extent, these rhythmical movements display the dynamical behavior of very simple limit cycles. The stability of the kinematics in the face of perturbation indicates that an attractor is present. The dimensionality results show that this attractor is of low dimension, not inconsistent with a one-dimensional limit cycle at the intermediate amplitude scales and stochastic noise at the smaller amplitude scales.

Many of the present results are consistent with a previously derived hybrid model (Kay et al., 1987). The hybrid oscillator is a combination of the van der Pol and Rayleigh oscillators:

$$m\ddot{x} + \alpha\dot{x} + \beta\dot{x}^3 + \gamma(x - x_0)^2\dot{x} + k(x - x_0) = 0, \quad (10)$$

where β is the coefficient of the Rayleigh nonlinear damping term (cf. Equation 2). Kay et al. found that this oscillator best modeled the covariation of frequency and amplitude of wrist movements in the unperturbed case. In the present data set, the observed relaxation time is a function of the magnitude of perturbation only and was constant across movement frequency, as predicted by the hybrid model. The attractor strength is also constant across movement frequency, also as predicted by the hybrid model. A further agreement with this model is the spectra of the steady-state trials. The harmonic structure of the hybrid (as well as the van der Pol and Rayleigh) oscillators contains only every other harmonic for a wide range of attractor strength. Although our movement data exhibited both even and odd harmonics, the observed pattern—with the even harmonic F_2 relatively attenuated compared with the odd harmonic F_3—was similar in form to the harmonic structure of these simple nonlinear oscillators.

However, there are two discrepancies between the model and the present data, both of which were revealed by perturbation. First, the movement's strength of attraction is non-uniform on the phase plane, unlike the hybrid model. Thus, the behavior of the movement when it is not on the limit cycle is different from that of the model.

[3] We also performed the computation on simulated data consisting of a digitally generated sine wave with added quasi-random noise; ν converged to a value of 1.267, with some variability in the next significant digit.

Second, the observed pattern of phase response differs from the pattern predicted by the hybrid or similar oscillators. Although these oscillators can be phase shifted by mechanical perturbation at particular old phases, they do not exhibit an overall phase shift when averaged across all possible old phases. The model of mechanical perturbation to the hybrid oscillator, for example, is as follows: When the perturbation is off, the equation of motion is Equation 10. When the perturbation is on, a torque pulse is added as a forcing function:

$$m\ddot{x} + \alpha\dot{x} + \beta\dot{x}^3 + \gamma(x - x_0)^2\dot{x} + k(x - x_0) = \Gamma. \quad (11)$$

In effect, the perturbation serves only to reset the initial conditions, that is, the mechanical state of the system, to effectively new starting values. For small Γ, the postperturbation initial conditions are only slightly different from the preperturbation locus, and the phase shift produced for any particular old phase (ϕ) is small, diverging only slightly from the $\phi = \phi'$ line. Consider one direction of perturbation: Suppose Γ is positive, and, in a model of our rhythmic movements, corresponds to extension pulses. In the oscillator's "extension" half-cycle, Γ has the effect of speeding up the motion, because it is in the direction of motion and so assists it in getting to peak extension. Thus, in this half-cycle, the hybrid oscillator is phase-advanced by an extension pulse. In the flexion half-cycle, an extension pulse has the effect of slowing down the motion, because it is in the direction opposite to the motion, holding it back from peak flexion. In this half-cycle, the oscillator is phase-delayed by an extension pulse. With uniform sampling of perturbation phase over the entire cycle, these effects balance exactly, and no average phase shift results whatsoever (see Figure 10).

Thus, when the PTC for the hybrid is fitted across all possible perturbation phases, the intercept is always nonsignificant for small perturbations, in contrast to the significant positive intercepts found in the present data.[4] In addition, the phase-dependent pattern of phase shift for the hybrid oscillator is quite different from the observed data: Instead of two peaks at roughly halfway through the extension and flexion half-cycles, this oscillator's PTC exhibits a peak during the extension half-cycle and a trough during the flexion half-cycle, for extension pulses. The pattern of advances and delays is reversed for flexion pulses ($\Gamma < 0$), but, again, the overall phase shift is zero and only one peak occurs in the PTC.

It seems likely, therefore, that second-order, time-invariant dynamical systems may be inadequate for capturing the patterns of phase response of our movement data. One possibility is to modify the assumption of time invariance: Perhaps, in addition to transiently affecting the mechanical state of the system (which it surely does), the perturbation has an additional transient effect on the system's parameters.

The overall phase advance we observed indicates that, on average, the movement temporarily speeds up in response to the perturbation. This would occur if the stiffness of the movement system temporarily increases, either during the perturbation itself or for a short period of time afterward, or both. Stiffening up the hybrid oscillator leads to the following equation of motion for the duration of the perturbation:

$$m\ddot{x} + \alpha\dot{x} + \beta\dot{x}^3 + \gamma(x - x_0)^2\dot{x} + k(\Gamma)(x - x_0) = \Gamma, \quad (12)$$

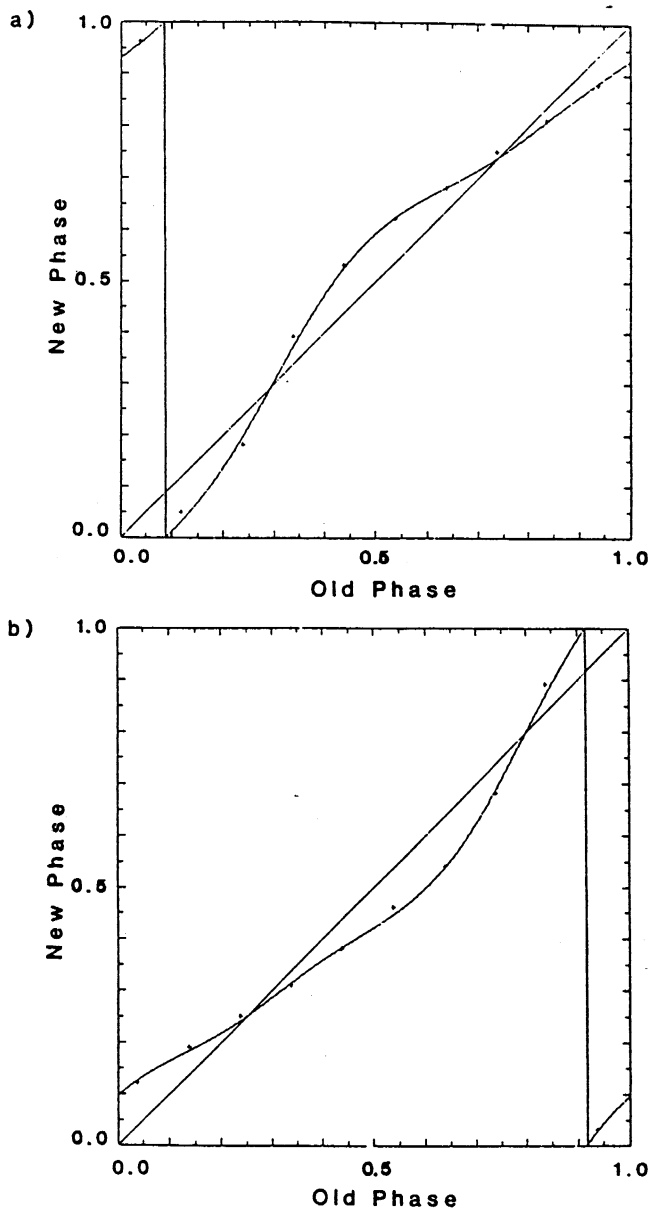

Figure 10. Phase transition curve (ϕ vs. ϕ') of the simulated hybrid oscillator, perturbed with (a) weak extension and (b) weak flexion torque pulses.

where k is now a function of the perturbation. In order to match the experimental results, this stiffening function should be independent of both magnitude and direction of the torque pulse (Γ), and so may be written as

$$\begin{aligned} k &= k_0, && \text{when } \Gamma = 0 \\ &= k_0 + \Delta k, && \text{when } \Gamma \neq 0, \end{aligned} \quad (13)$$

where k_0 is the stiffness during steady-state portions, and Δk is some positive number. This model's PTC has an overall phase advance, but it has the same phase-dependent pattern

[4] For larger perturbations, the hybrid, van der Pol, and Rayleigh oscillators exhibit Type 0 phase resetting.

of phase shift (one maximum and one minimum) as the hybrid in Equation 11. In order to match the data's phase-dependent pattern, we must choose another stiffness function, and it may have to be a radically different one. It is also possible, of course, that the hybrid is simply the wrong candidate dynamical system, and other systems of different structure or higher order are required to model our data.

One example is composed of two oscillatory components: a central nervous system oscillator driving a peripheral limb segment with its own oscillatory biomechanical dynamics. Counting each oscillatory component as a second-order process, this situation would be described by a fourth-order system of differential equations. Our results suggest that if this model is to be taken seriously, the central oscillator is not independent of the limb's dynamics (Grillner, 1981; Saltzman & Kelso, 1987; Turvey, Rosenblum, Schmidt, & Kugler, 1986; Wing, 1980). If there is a central timekeeper, it is affected by perturbations delivered to the limb being controlled. In other words, the coupling between the central timer and the peripheral musculo-skeletal oscillator is fundamentally bidirectional, not unidirectional. Explicit central pattern generator models for this activity must, therefore, include feedback from the peripheral, controlled system.[5]

In summary, we have obtained a fairly complete characterization of the dynamical behavior of a simple rhythmical voluntary movement. Many of these characteristics agree quite closely with simple one-dimensional limit-cycle dynamics. However, certain aspects of the present data set do not, and work remains to be done to understand these differences. The present data set constrains the form that any model of this type of behavior might assume; some classes of dynamics (e.g., some forms of second-order dynamics with time-invariant parameterizations) have been excluded as possible models. It remains to be seen whether these results generalize to different classes of rhythmic movement—for example, involuntary tremor oscillations or multijoint and multilimb tasks—or whether, in those instances, qualitatively different dynamics prevail.

[5] It is interesting to note that Lennard (1985) reached a similar conclusion in his study of perturbed monopodal swimming movements in the turtle. In perturbing the turtle triceps muscle nerve, he obtained a consistent phase shift, also a phase advance, but for only two phases of perturbation. Intriguingly, these phases (at $\phi = 0.25$ and $\phi = 0.85$) correspond roughly to the points of maximum phase shift found in our experiment.

References

Abraham, N. B., Albano, A. M., Das, B., de Guzman, G., Yong, S., Gioggia, R. S., Puccioni, G. P., & Tredicce, J. R. (1986). Calculating the dimension of attractors from small data sets. *Physics Letters, 114A*, 217–221.

Abraham, R. H., & Shaw, C. D. (1982). *Dynamics—The geometry of behavior*. Santa Cruz, CA: Ariel Press.

Andronov, A., & Chaikin, C. E. (1949). *Theory of oscillations*. Princeton, NJ: Princeton University Press.

Bergé, P., Pomeau, Y., & Vidal, C. (1984). *Order within chaos: Towards a deterministic approach to turbulence*. New York: Wiley.

Carpenter, G. A., & Grossberg, S. (1983). A neural theory of circadian rhythms: The gated pacemaker. *Biological Cybernetics, 48*, 35–59.

Fraser, A. M., & Swinney, H. L. (1986). Independent coordinates for strange attractors from mutual information. *Physical Review A, 33*, 1134–1140.

Grassberger, P., & Procaccia, I. (1983). Measuring the strangeness of strange attractors. *Physica, 9D*, 189–208.

Grillner, S. (1981). Control of locomotion in bipeds, tetrapods, and fish. In J. M. Brookhart & V. B. Mountcastle (Eds.), *Handbook of physiology, Section 1: The nervous system. Vol. II: Motor control, Part 1* (pp. 1179–1236). Bethesda, MD: American Physiological Society.

Grillner, S., & Zangger, P. (1979). On the central generation of locomotion in the low spinal cat. *Experimental Brain Research, 34*, 241–262.

Holzfuss, J., & Mayer-Kress, G. (1986). An approach to error-estimation in the application of dimension algorithms. In G. Mayer-Kress (Ed.), *Dimensions and entropies in chaotic systems: Quantification of complex behavior* (pp. 114–122). New York: Springer-Verlag.

Jordan, D. W., & Smith, P. (1977). *Nonlinear ordinary differential equations*. Oxford, England: Clarendon.

Kay, B. A. (1988). The dimensionality of movement trajectories and the degrees of freedom problem: A tutorial. *Human Movement Science, 7*, 343–364.

Kay, B. A., Kelso, J. A. S., Saltzman, E. L., & Schöner, G. (1987). The space–time behavior of single and bimanual rhythmical movements: Data and model. *Journal of Experimental Psychology: Human Perception and Performance, 13*, 178–192.

Kay, B. A., Munhall, K. G., V.-Bateson, E., & Kelso, J. A. S. (1985). A note on processing kinematic data: Sampling, filtering, and differentiation. *Haskins Laboratories Status Report on Speech Research, SR-81*, 291–303. New Haven, CT: Haskins Laboratories.

Kelso, J. A. S., Holt, K. G., Rubin, P., & Kugler, P. N. (1981). Patterns of human interlimb coordination emerge from the properties of non-linear limit-cycle oscillatory processes: Theory and data. *Journal of Motor Behavior, 13*, 226–261.

Kerlinger, F. N., & Pedhazur, E. J. (1973). *Multiple regression in behavioral research*. New York: Holt, Rinehart & Winston.

Kugler, P. N., & Turvey, M. T. (1987). *Information, natural law, and the self-assembly of rhythmic movement*. Hillsdale, NJ: Erlbaum.

Kugler, P. N., Turvey, M. T., Schmidt, R. C., & Rosenblum, L. D. (1990). Investigating a nonconservative invariant of motion in coordinated rhythmic movements. *Ecological Psychology, 2*, 151–189.

Lennard, P. (1985). Afferent perturbations during "monopodal" swimming movements in the turtle: Phase-dependent cutaneous modulation and proprioceptive resetting of the locomotor rhythm. *Journal of Neuroscience, 5*, 1434–1445.

Mandelbrot, B. B. (1983). *The fractal geometry of nature*. San Francisco: Freeman.

Mayer-Kress, G. (Ed.). (1986). *Dimensions and entropies in chaotic systems: Quantification of complex behavior*. New York: Springer.

Mayer-Kress, G., & Layne, S. (1987). Dimensionality of the human electroencephalogram. In S. H. Koslow, A. J. Mandell, & M. F. Shlesinger (Eds.), *Proceedings of the New York Academy of Sciences Conference on Perspectives in Biological Dynamics & Theoretical Medicine* (pp. 62–87). New York: New York Academy of Sciences.

Minorsky, N. (1974). *Nonlinear oscillations*. New York: Krieger.

Pittendrigh, C. S., & Daan, S. (1976). A functional analysis of circadian pacemakers in nocturnal rodents: IV. Entrainment: Pacemaker as clock. *Journal of Comparative Physiology, 106*, 291–336.

Saltzman, E. L., & Kelso, J. A. S. (1987). Skilled actions: A task dynamic approach. *Psychological Review, 94*, 84–106.

Selverston, A. I. (1980). Are central pattern generators understand-

able? *Behavioral and Brain Sciences, 3,* 535–571.

Stein, P. S. G. (1976). Mechanisms of interlimb phase control. In R. N. Herman, S. Grillner, P. S. G. Stein, & D. G. Stuart (Eds.), *Neural control of locomotion* (pp. 465–487). New York: Plenum Press.

Thompson, J. M. T., & Stewart, H. B. (1986). *Nonlinear dynamics and chaos: Geometrical methods for engineers and scientists.* New York: Wiley.

Turvey, M. T., Rosenblum, L. A., Schmidt, R. C., & Kugler, P. N. (1986). Fluctuations and phase in coordinated rhythmic movements. *Journal of Experimental Psychology: Human Perception and Performance, 12,* 564–583.

van der Pol, B. (1926). On relaxation-oscillations. *Philosophical Magazine, 7,* (2), 978–992.

Winfree, A. T. (1980). *The geometry of biological time.* New York: Springer.

Wing, A. M. (1980). The long and short of timing in response sequences. In G. E. Stelmach & J. Requin (Eds.), *Tutorials in motor behavior* (pp. 469–486). *Amsterdam: North-Holland.*

Yamanishi, J., Kawato, M., & Suzuki, R. (1979). Studies on human finger tapping neural networks by phase transition curves. *Biological Cybernetics, 33,* 199–208.

Appendix

Derivation of a Measure of Limit-Cycle Attractor Strength

Assume that the return to the limit cycle following perturbation is a linear relaxation process in amplitude only; that is, the return trajectory spirals back to the limit cycle, with the radial displacement from the limit cycle decaying exponentially back. Let

$$r'(t) = r(t) - r_L(t), \tag{A1}$$

where $r(t)$ is the radial displacement of the return trajectory at time t from the center of oscillation and $r_L(t)$ is the radial displacement of the limit cycle from the center of oscillation at the same phase angle of the return trajectory at time t. The assumption of linear relaxation can now be explicitly written as

$$\frac{dr'}{dt} = -\sigma r'. \tag{A2}$$

Integration gives the solution:

$$r'(t) = r'(0)e^{-\sigma t}, \tag{A3}$$

where $r'(0)$ is the displacement from the limit cycle at $t = 0$. Solving for σ gives

$$\sigma = -\frac{1}{t} \ln \left| \frac{r'(t)}{r'(0)} \right| \tag{A4}$$

or

$$\sigma = \frac{1}{t} ln \left| \frac{r(0) - r_L(0)}{r(t) - r_l(t)} \right|, \tag{A5}$$

where ln is the natural algorithm function. The σ can be measured any time after the perturbation is turned off, but for practical purposes, some end to the return process must be defined. Under the decay assumption, the computation is valid for trajectories starting both outside and inside the limit cycle. Also, the return process takes an infinite amount of time, but a real return would be buried in the variation of the observed behavior after some finite time. Furthermore, the computation is valid only when the numerator in the argument of the logarithmic function is larger than the denominator. Note that the σ in this article corresponds to α/m in Equation A9 in Kay et al. (1987). That is, it represents the relaxation constant of the linearized return process of the van der Pol oscillator, normalized to unit mass. The return processes of the van der Pol, Rayleigh, and hybrid oscillators are all nonlinear (Jordan & Smith, 1977). They are more nonlinear given larger nonlinear damping terms and greater distances from the limit cycle. We have chosen to assume linearity to simplify the extraction of our attractor strength measure.

Received January 25, 1989
Revision received February 26, 1990
Accepted February 27, 1990 ■